Langmuir
Article
pubs.acs.org/Langmuir
© 2010 American Chemical Society

Dynamic Angular Segregation of Vesicles in Electrohydrodynamic Flows

William D. Ristenpart,*,† Olivier Vincent,‡,⊥ Sigolene Lecuyer,‡ and Howard A. Stone‡,§

†Department of Chemical Engineering & Materials Science and Department of Food Science & Technology, University of California at Davis, Davis, California 95616, and ‡School of Engineering & Applied Sciences, Harvard University, Cambridge, Massachusetts 02138. §Current address: Department of Mechanical and Aerospace Engineering, Princeton University, Princeton, NJ 08544. ⊥Current address: Laboratoire de Spectrométrie Physique, CNRS & Grenoble Universités, BP 87, 38402 St. Martin d'Hères Cedex, France

Received January 29, 2010. Revised Manuscript Received March 29, 2010

We investigate a new type of behavior whereby small vesicles orbiting around a larger vesicle in a toroidal electrohydrodynamic flow undergo dynamic angular segregation. Application of a low frequency (~50 Hz) electric field induces aggregation of adjacent unilamellar vesicles near the electrode, in a manner similar to that observed with rigid colloidal particles. For polydisperse vesicle suspensions, however, small vesicles (< 10 μm) are often observed to "orbit" around larger vesicles (> 20 μm) in a toroidal electrohydrodynamic flow field. While orbiting, the smaller vesicles gradually segregate into well-defined angular cross sections. Viewed from above, the vesicles appear to form dynamic "bands" at prescribed angles, separated by regions devoid of vesicles. We interpret the angular segregation in terms of induced dipolar interactions, and we propose a model based on point dipoles rotating in a cellular flow field. We demonstrate that the model yields a surprisingly diverse range of vesicle trajectories, including many that are qualitatively consistent with the experimental observations.

Introduction

Electrohydrodynamic (EHD) flows,[1] also known as induced-charge electroosmotic flows,[2] are known to cause colloidal particles to aggregate near electrodes.[3,4] The applied electric field polarizes the colloidal particles, and the dipole field around each colloid generates a tangential electric stress in the charge polarization layer near the electrode. This stress generates a toroidal EHD flow field around each colloid (cf. Figure 1A), and adjacent particles are mutually entrained in their respective flow fields, resulting in planar aggregation on the electrode. Because the particle dipole field and the charge density in the electrode polarization layer both scale with the magnitude of the applied field E, the resulting EHD flow typically scales as the square of the applied field.[3,4] The generation of an EHD flow around colloids near electrodes has been investigated under many different circumstances, and we refer the interested reader to the work by Saville and colleagues[5,6] or by Hoggard et al.[7] for examples and references therein.

Almost all of the experimental work to date, however, has focused on rigid and monodisperse colloidal particles. We recently demonstrated[8] that similar EHD flow and aggregation also occurs around unilamellar phospholipid vesicles, which are self-assembled, spherical molecular bilayers that separate a well-defined internal volume from the external environment. In our case we generated vesicles via electroformation, yielding vesicle diameters ranging from approximately 1 to 50 μm. Although the vesicles are filled with an aqueous solution, the presence of the membrane allows accumulation of charge and the consequent establishment of a dipolar field around the vesicle, thereby inducing EHD flows along the electrode in the same manner as solid colloids. Unlike previous observations with solid colloids, however, the behavior of the vesicles was highly sensitive to the size of adjacent vesicles. For similarly sized vesicles, they simply aggregated along the electrode into planar clusters in the same manner as observed for monodisperse colloids. For sufficiently large size disparity, though, one of two behaviors was observed: lifting or orbiting. In the lifting behavior, the smaller vesicles (< ~10 μm) tended to aggregate into clusters underneath a larger vesicle (> 20 μm), thereby "lifting" the large vesicle away from the electrode. We demonstrated[8] that this behavior could be exploited to effectively separate the largest vesicles preferentially from the smaller ones, something which is difficult to do by conventional methods (e.g., filtration or centrifugation) because of the fragility of the vesicles.

Oftentimes, however, we observed the "orbiting" behavior, which was characterized by the smaller vesicles moving in well-defined circulatory "orbits" around the larger vesicle (Figure 1a). Qualitatively, it appeared that the smaller vesicles were following the EHD streamlines induced by the larger vesicle, but surprisingly the smaller vesicles tended to align at preferred azimuthal angles. Although the vesicles continued to circulate with the EHD flow (i.e., in the poloidal direction), large regions became depleted of vesicles. Viewed from above, the vesicles appeared to form dynamic "bands" orbiting at prescribed azimuthal orientations. It was unclear why they should form bands, and it was unclear why occasionally a set of orbiting vesicles would suddenly and simultaneously move underneath the larger vesicle, thereby lifting it up. Since the orbiting behavior is undesirable in regard to maximizing the separation efficiency, we sought to understand why the vesicles undergo orbiting versus lifting.

The main goal of this paper is to demonstrate that the angular segregation observed during orbiting is explicable in terms of a competition between drag induced by the EHD flow and dipolar

*Corresponding author. E-mail: wdristenpart@ucdavis.edu.
(1) Saville, D. A. *Annu. Rev. Fluid Mech.* **1997**, *29*, 27–64.
(2) Squires, T. M.; Bazant, M. Z. *J. Fluid Mech.* **2004**, *509*, 217–252.
(3) Trau, M.; Saville, D. A.; Aksay, I. A. *Science* **1996**, *272*, 706–709.
(4) Trau, M.; Saville, D. A.; Aksay, I. A. *Langmuir* **1997**, *13*, 6375–6381.
(5) Ristenpart, W. D.; Aksay, I. A.; Saville, D. A. *Phys. Rev. E* **2004**, *69*, 021405.
(6) Ristenpart, W. D.; Aksay, I. A.; Saville, D. A. *J. Fluid Mech.* **2007**, *575*, 83–109.
(7) Hoggard, J. D.; Sides, P. J.; Prieve, D. C. *Langmuir* **2008**, *24*, 2977–2982.
(8) Lecuyer, S.; Ristenpart, W. D.; Vincent, O.; Stone, H. A. *Appl. Phys. Lett.* **2008**, *92*, 104105.

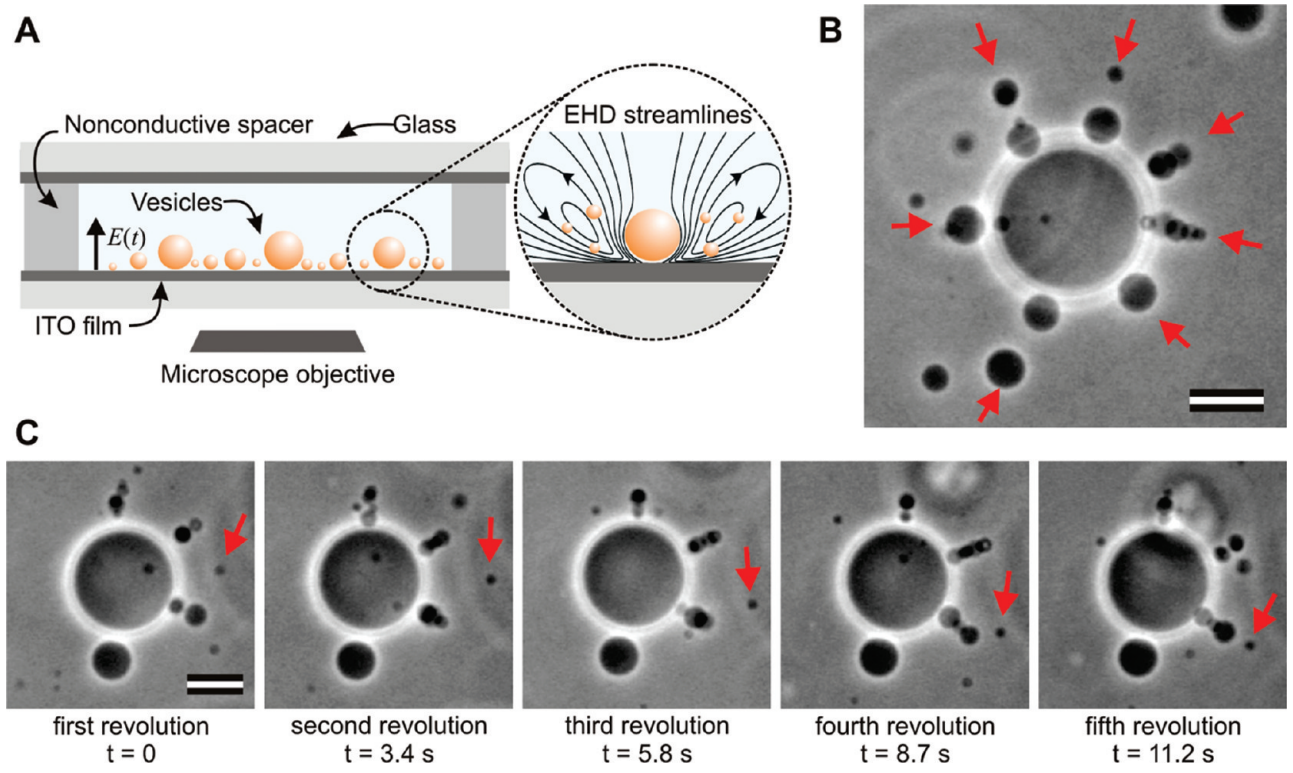

Figure 1. Experimental observations of dynamic angular segregation. (A) Sketch of the experimental apparatus (not to scale). The magnification shows a qualitative sketch of the toroidal EHD streamlines induced around a large vesicle. (B) Optical micrograph showing a projected (plan) view of the dynamic bands of smaller vesicles orbiting around a larger vesicle in center. The arrows denote the approximate position of the bands, each of which consists of multiple vesicles rotating around each other. Image taken from Supporting Information movie 1. Electric field is 6 V, 100 Hz; scale bar is 25 μm. (C) Time lapse images showing an individual vesicle (denoted by the arrow) moving to join one of the bands. During each revolution it moves slightly closer to the band at lower right. Images taken from Supporting Information movie 2. Electric field is 8 V, 100 Hz; scale bar is 20 μm.

interactions between the orbiting vesicles. Toward this end, we develop a simplified model that approximates the vesicles as point dipoles moving in a cellular flow field. Despite the simplicity of the model, a strikingly diverse collection of steady-state trajectories is observed, and several of the calculated trajectories mimic those observed experimentally.

The paper is organized as follows. We begin by briefly describing the experimental observations, and then we develop a two-dimensional model for the case of two point dipoles interacting in a cellular flow field. Their behavior is mapped for a wide range of dimensionless parameter space, and we use those results to expand the model to interactions between N point dipoles in a full three-dimensional toroidal flow field. The key result is that for some range of dimensionless parameters the dynamic angular segregation is replicated numerically. We conclude by discussing possibilities for improving the model with the ultimate goal of learning how to improve the efficiency of size separation of vesicles by EHD methods.

Experimental Observations

Our experimental apparatus and procedure for fabricating vesicles have been described previously.[8] Briefly, a polydisperse suspension of dioleoylphosphatidylcholine (DOPC) giant unilamellar vesicles was prepared using a standard electroformation procedure[9] to generate 0.1 M sucrose-filled GUVs suspended in 0.1 M glucose solution. A small volume of the vesicle solution was transferred into the chamber of the device sketched in Figure 1, which consisted of two parallel glass slides (2 mm separation) coated with ITO (R_s = 4−8 ohm/square) that served as electrodes. Oscillatory electric fields were applied between the electrodes using a function generator, and the resulting vesicle motion was observed with a phase-contrast microscope.

Upon application of a sufficiently strong potential difference (> 1 V) and sufficiently low frequency (between 10 and 100 Hz), similarly sized vesicles proceeded to aggregate. Vesicles with sufficient size disparity, however, exhibited either the lifting or orbiting behavior. The lifting behavior has already been described in more detail previously;[8] here we focus on the orbiting behavior, examples of which are shown in Figure 1b,c and in Supporting Information movies 1 and 2. Typically, a large vesicle (> 20 μm) would attract a crowd of smaller vesicles (< 10 μm) that would begin to move periodically toward and away from the larger vesicle. Because the orbiting vesicles moved slightly in and out of focus during each revolution, it was clear that they were moving vertically as well as horizontally during each revolution, in a manner at least qualitatively consistent with the streamlines sketched in Figure 1a.

Most striking, however, was the tendency for the orbiting vesicles to align along preferred orientations. Note that the vesicles were initially randomly dispersed along the electrode, and upon application of the field the small vesicles sufficiently close to a large vesicle simply began orbiting at an angle prescribed by their initial position. Over the course of several revolutions, however, the small vesicles moved onto trajectories closer to one another, ultimately forming "bands" similar to those shown in Figure 1b. We emphasize that these bands are dynamic, with individual vesicles occasionally joining or (much less frequently) leaving. A specific example of the band formation process is shown in Figure 1c, which tracks a single small vesicle as it migrates closer to a band over the course of five revolutions (cf. Supporting Information movie 2). Note that the dominant

(9) Angelova, M. I.; Dimitrov, D. S. *Faraday Discuss.* **1986**, *81*, 303.

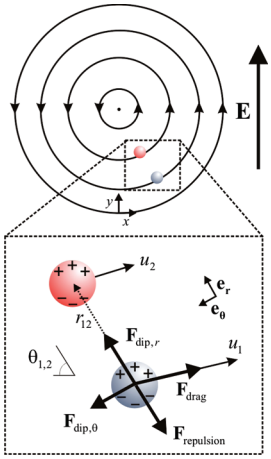

Figure 2. Sketch of the forces acting on two electrically polarized objects moving in a circular flow.

force acting on the smaller vesicle is clearly the drag force due to the EHD flow, since the smaller vesicle continues to move periodically toward and away from the larger vesicle, while a weaker but non-negligible force tends to draw the smaller vesicle toward a nearby band over the time scale of multiple revolutions.

During the course of an experiment, typically about half of the large vesicles attracted crowds of orbiting small vesicles, while the other half simply lifted up on top of a layer of smaller vesicles. Over time, some of the orbiting vesicles would cease orbiting and accumulate underneath the larger vesicle, thereby lifting it off. Because the dynamics are complex, we now turn to modeling efforts to attempt to shed some light on the observed behavior.

Theory: Point Dipoles in a Cellular Flow

The preceding experiments demonstrate that the electric field causes the vesicles to align preferentially along certain angles (i.e., form bands). The next question is: why? Many electrically induced behaviors observed with rigid colloids have been interpreted in terms of dipolar interactions,[10−13] which tend to cause the particles to align with the field. The "pearl chains" formed in electrorheological fluids[10] are a well-known example of the consequence of dipolar interactions. Furthermore, note that the EHD flow itself is caused by the interaction between the dipole field and the free charge near the electrode.[5,6] Since the vesicles are clearly polarized (as evidenced by the generated EHD flow), we investigate here the hypothesis that the banding is similarly due to induced dipole−dipole interactions between the orbiting vesicles themselves. In previous work on induced dipolar interactions between colloids the surrounding fluid has either been quiescent or subject to linear shear, but here we are faced with the more complex situation of an EHD flow generated by the interaction of a large vesicle with the nearby electrode. We therefore begin by examining the interaction of just two polarized objects in a model flow field (Figure 2), before moving on to more complicated interactions.

Application of the external field causes each vesicle to polarize, and a useful model for the electric force exerted on adjacent polarized objects is the point-dipole model[14]

$$\mathbf{F}_{dip} = \frac{\beta(E,\omega,C_0,...)}{r_{ij}^4}\mathbf{f}(\theta_{ij}) \qquad (1)$$

where

$$\mathbf{f}(\theta_{ij}) = (3\cos\theta_{ij}^2 - 1)\mathbf{e}_r + \sin 2\theta_{ij}\,\mathbf{e}_\theta \qquad (2)$$

Here r_{ij} is the center-to-center separation between the vesicles, and θ_{ij} is the angle formed between the applied field and the vesicle line of centers. The unit normal vectors $\mathbf{e}_r$ and $\mathbf{e}_\theta$, in the radial and angular directions, respectively, are defined with respect to the ith vesicle (Figure 2). The prefactor $\beta(E,\omega,C_0,...)$ describes the magnitude of the force and depends among other variables on the magnitude E and frequency ω of the applied field, the object size, and the system material properties (such as permittivity and ionic strength). The influence of these latter parameters is captured in the dimensionless dipole coefficient C_0. Note that the force depends on the square of the applied field, E^2, while the frequency dependence is more complicated but is often described using the Maxwell−Wagner model.[10,11] A significant feature of eq 1 is that the dipolar interaction is highly anisotropic, as captured in the dimensionless vector $\mathbf{f}(\theta_{ij})$ given in eq 2. For dipoles aligned with the field ($\theta_{ij} = 0$ or 180°), the interaction is positive (attractive) and the dipoles tend to aggregate. In contrast, dipoles aligned perpendicular to the applied field ($\theta_{ij} = 90°$) experience a negative (repulsive) force and the dipoles tend to segregate. Moreover, the magnitudes of the respective forces are unequal since the radial component of the force is a factor of 2 greater for $\theta_{ij} = 0$ compared to $\theta_{ij} = 90°$.

The key implication of the point-dipolar interaction is that polarized objects at the same vertical distance above the electrode feel a repulsive interaction, while those at sufficiently different vertical distances feel an attractive interaction. Behavior consistent with this picture has been repeatedly observed in the context of rigid colloids, where most particles near the surface of the electrode repel (in the absence of EHD flow), but some fractions are observed to move up on top of other particles such that they are aligned with the field.[12,15] In the situation of interest here, however, the vesicles are continually moving in a toroidal flow field around a larger vesicle. Adjacent vesicles can therefore alternate between aligned and unaligned with respect to the applied field during the course of a single orbit, and a model of the flow field is necessary. Although detailed analytical models for the EHD flow field around a rigid spherical colloid are available,[6] the solutions depend on a truncated infinite series in bispherical coordinates. More importantly, necessary details about the electrokinetic properties of the vesicles are not well characterized, and the extant solutions do not incorporate the influence of the deformable vesicle interface.

Instead of addressing these complexities, we focus on a more fundamental question: what is the interaction behavior of polarized objects in a circulating flow? To address this question, we ignore most of the complexities listed above, and we present a simplified model focusing on the interactions of point dipoles in a cellular flow. As we shall demonstrate, this approach yields a surprisingly diverse set of trajectories, including many that qualitatively match the experimental observations.

The model description is as follows. First, we assume that the EHD flow structure around a large vesicle may be modeled by the cellular velocity field $\mathbf{u} = (u_x, u_y)$ defined by

$$u_x = U_0 \cos\lambda x \cos\lambda y, \quad u_y = U_0 \sin\lambda x \sin\lambda y \qquad (3)$$

Here U_0 is the magnitude of the flow velocity and λ^{-1} is the size of the cellular flow. Note that the velocity distribution has closed

(10) Gast, A. P.; Zukoski, C. F. *Adv. Colloid Interface Sci.* **1989**, *30*, 153–202.
(11) Parthasarathy, M.; Klingenberg, D. J. *Mater. Sci. Eng., R* **1996**, *17*, 57–103.
(12) Gong, T. Y.; Wu, D. T.; Marr, D. W. M. *Langmuir* **2002**, *18*, 10064–10067.
(13) Gong, T. Y.; Wu, D. T.; Marr, D. W. M. *Langmuir* **2003**, *19*, 5967–5970.
(14) Jackson, J. D. *Classical Electrodynamics*, 2nd ed.; John Wiley & Sons: New York, 1975.
(15) Ristenpart, W. D.; Aksay, I. A.; Saville, D. A. *Phys. Rev. Lett.* **2003**, *90*, 128303.

streamlines. Similar flow fields have previously been used to model the motions of aerosols and particles moving through cellular periodic flows.[16−20] Although the flow specified by eq 3 extends through all space with periodically arranged counter-rotating cells, we restrict attention to a single cell, i.e., the region $-\pi/2 < \lambda x < \pi/2$ and $0 < \lambda y < \pi$. The velocity profile thus mimics a cross section of the toroidal EHD flow around a large vesicle. Although this model does not capture the more complicated flow structure due to the presence of the large vesicle, it does share the essential feature of a circulatory flow. Note that we have assumed that any EHD flow generated by the smaller vesicles is negligible. To mimic the full three-dimensional toroidal flow, we specify the velocity field as $\mathbf{u} = (u_x, u_y, 0)$, i.e., with u_x and u_y given by eq 3 and zero imposed velocity in the z-direction. Periodic boundary conditions are then specified at $z = 0$ and $z = L$, where L is the circumference of the large vesicle inducing the EHD flow. For sufficiently large L, the resulting flow structure mimics the toroidal flow.

Next, we examine the interactions between the smaller vesicles as they move about in the cellular flow (eq 3). For sufficiently small values of U_0, the Reynolds number is small and viscous drag is dominant. Since vesicles are deformable, the drag force they experience is nontrivial, but in this model we ignore this complexity. We therefore assume that the hydrodynamic force on an individual particle is given by Stokes drag

$$F_D = 6\pi\mu a \frac{d\mathbf{x}}{dt} \tag{4}$$

where μ is the viscosity, a is the vesicle size, and $\mathbf{x}$ is the position vector of the center of mass of the vesicle. By Faxen's law, to leading order the trajectory of the ith vesicle in the flow field is given by

$$6\pi\mu a \frac{d\mathbf{x}_i}{dt} = 6\pi\mu a\mathbf{u} + \sum_j \mathbf{F}_{E,j} \tag{5}$$

where $\mathbf{F}_{E,j}$ represents all of the electrical forces acting on the ith vesicle. Here we have neglected higher order corrections in Faxen's law (i.e., the particles do not disturb the background flow) which limits the model to situations where $\lambda a \ll 1$. Higher-order drag effects, wall effects, and hydrodynamic interactions between vesicles are also neglected.

The electrical forces are, in general, comprised of several different effects, including electrophoretic motion due to charge on the vesicles, dielectrophoretic motion due to any nonuniformity in the field, and induced−induced dipolar interactions between vesicles. For the oscillatory fields of interest here, we assume that the frequency is sufficiently high that electrophoretic motion is negligible. Moreover, as a first approximation we ignore the nonuniform electric field due to the presence of the large vesicle that generates the toroidal EHD flow, so the electric field is simply $\mathbf{E} = E_\infty \mathbf{e}_y$. These assumptions leave the induced dipolar interaction as the primary consequence of the external electric field, so by the point-dipole approximation the force on the ith vesicle is given by eq 1. Note that the representation of the vesicles as point dipoles is consistent with the neglect of higher-order hydrodynamic interactions.

The point-dipole representation, however, leads to difficulties because the dipolar force diverges as $r_{ij} \to 0$. Physically, the finite size of the vesicles and the corresponding colloidal interactions (i.e., the electrostatic repulsion between diffuse charge layers) prevent two adjacent vesicles from interpenetrating. This interaction is typically represented with the standard DLVO model, which has a repulsive component that decays exponentially with a characteristic length scale given by the Debye length.[21] The DLVO model, however, is invalid in the limit of point dipoles, since an exponential decay (which converges to unity as $r \to 0$) is necessarily weaker than the divergent power-law decay described by eq 1. Hence, the standard DLVO model does not prevent divergent interactions, and a different description for point dipoles is necessary.

To approximate the repulsive interactions in a manner consistent with the point-dipolar representation, we define a "pseudo-hard-sphere" repulsion

$$\mathbf{F}_{rep} = -\frac{\xi}{r_{ij}{}^m}\mathbf{e}_r \tag{6}$$

Here the parameter ξ represents the magnitude of the repulsive interaction and thus depends on the radius of the vesicle, while the exponent m controls how rapidly the repulsion decays with distance. Provided $m > 4$ so that divergent interactions are prevented, we are free to choose any value for m; higher values of m yield a steeper repulsive barrier and are thus more "hard-sphere-like". In the numerical calculations described below, we chose $m = 13$, which mimics the Lennard-Jones repulsive force valid on molecular length scales. We emphasize that we are not claiming that an r^{-13} repulsive interaction is present physically in the experiments described above; rather, this description merely serves as a generic repulsive force for our numerical calculations. Other values of m are equally "valid", and as we shall see the general behavior observed is not sensitive to the specific choice of m.

Combining eqs 1, 3, 5, and 6, we find that the position of each particle is governed in dimensionless terms by

$$\frac{d\hat{\mathbf{x}}_i}{d\tau} = \hat{\mathbf{u}}(\hat{\mathbf{x}}_i) + \sum_{i\neq j}\left[\frac{N_{dip}}{\rho_{ij}{}^4}\mathbf{f}(\theta_{ij}) - \frac{N_{rep}}{\rho_{ij}{}^{13}}\mathbf{e}_r\right] \tag{7}$$

Here we have defined the dimensionless parameters

$$\tau \equiv tU_0\lambda \tag{8}$$

$$\rho_{ij} \equiv r_{ij}\lambda \tag{9}$$

$$N_{dip} \equiv \frac{\beta(E,\omega,C_0,...)\lambda^4}{6\pi\mu a U_0} \tag{10}$$

$$N_{rep} \equiv \frac{\xi\lambda^{13}}{6\pi\mu a U_0} \tag{11}$$

where distance is scaled on the length scale of the circulating flow, λ^{-1}, while time is scaled on the characteristic time required for the fluid to make a revolution, $(U_0\lambda)^{-1}$. The dimensionless parameters N_{dip} and N_{rep} gauge respectively the relative magnitudes of the dipolar interaction and the repulsive interaction compared with the drag. In the limit where N_{dip} and N_{rep} are both zero, the particles simply follow the streamlines; the trajectories deviate from the streamlines when N_{dip} and/or N_{rep} is nonzero. For sufficiently strong dipolar interactions the objects will simply align with the field and not move much in response to the flow. Our experimental observations, however, suggest that neither effect is negligible, since the vesicles tend to align with the field while still undergoing pronounced recirculation, and we are therefore most interested

(16) Moffatt, H. K. *Rep. Prog. Phys.* **1983**, *46*, 621–664.
(17) Maxey, M. R. *Phys. Fluids* **1987**, *30*, 1915–1928.
(18) Dungan, S. R.; Brenner, H. *Phys. Rev. A* **1988**, *38*, 3601–3608.
(19) Druzhinin, O. A. *Phys. Fluids* **1995**, *7*, 2132–2142.
(20) Festa, R.; Mazzino, A.; Todini, M. *Phys. Rev. E* **2009**, *80*, 035301.

(21) Russel, W. B.; Saville, D. A.; Schowalter, W. R. *Colloidal Dispersions*, 1st ed.; Cambridge University Press: Cambridge, UK, 1991.

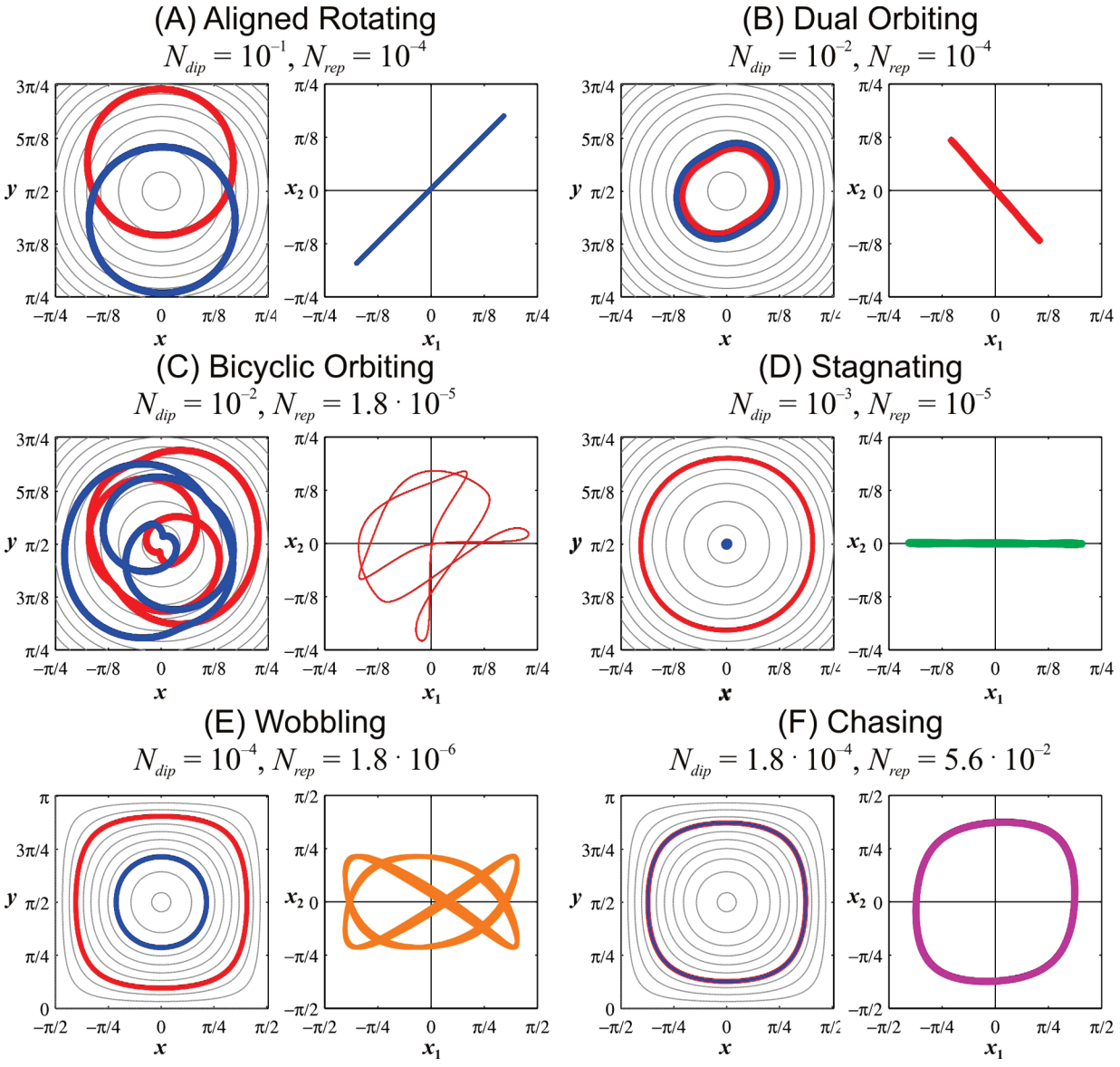

Figure 3. Representative trajectories (on left) and corresponding phase plots (on right) for two point dipoles moving in a cellular flow field, calculated by solving eq 7 numerically. The initial positions are identical in each case: $(x_1, y_1) = (\pi/2, \pi/4)$ and $(x_2, y_2) = (\pi/2, 0)$. The parameters N_{dip} and N_{rep} are specified as indicated in each case. In trajectories, particle 1 is red and particle 2 is blue; colors in phase plots correspond to those used in Figure 4. See also Supporting Information movies 3−8.

in the intermediate case where both drag and dipolar attraction are non-negligible. Substitution of characteristic values[23] into eq 10 yields $N_{dip} \approx 2 \times 10^{-2}$, while requiring that the dipolar attraction and pseudo-hard-sphere repulsion must balance at $r = 2a$ (cf. eq 12) yields $N_{rep} \approx 5 \times 10^{-5}$. As we shall see, simulations using parametric values close to these estimates yields behavior similar to that observed experimentally. Because eq 7 is nonlinear, we turn to numerical calculations to determine the particle trajectories for arbitrary values of N_{dip} and N_{rep}.

Two-Dimensional Numerical Simulations

For each simulation, specific values of N_{dip} and N_{rep} were chosen and initial dimensionless positions $(\hat{x}_{init}, \hat{y}_{init})$ for each of N particles were specified. (For simplicity, we henceforth omit the hat symbols and note that all values are dimensionless.) Equation 7 was then solved using standard numerical procedures (specifically, by means of the ode23 function in Matlab version 7.3). We first summarize key aspects of the behavior with just a pair of particles ($N = 2$) moving only in two dimensions, before addressing multibody effects in the full toroidal (three-dimensional) flow field.

Representative "steady-state" periodic trajectories for six basic types of behavior are shown in Figure 3. In each calculation, the point dipoles moved around transiently before obtaining a "steady-state" trajectory, here defined as a repetition of trajectory with less than 0.1% deviation, which typically occurred for $\tau \ll 10^3$. For each of the six behaviors, the left-hand plot shows the trajectory (y versus x for both dipoles), while the right-hand plot shows the "phase plot" of one x-coordinate versus the other). The initial dimensionless positions for the two point dipoles were $(x_1, y_1) = (\pi/2, \pi/4)$ and $(x_2, y_2) = (\pi/2, 0)$ in each calculation, so as

(22) Weisstein, E. W. Epitrochoid. http://mathworld.wolfram.com/Epitrochoid.html.

(23) Noting that $\beta = 12\pi\varepsilon\varepsilon_0 a^6 C_0^2 E^2$ for point dipoles,[11] where the dipole coefficient C_0 is order one, we substitute characteristic values from our experiments: $\varepsilon \approx 80$, $a \approx 5$ μm, $u \approx 10$ μm/s, $\mu \approx 10^{-3}$ kg/(m s), $\lambda \approx 5 \times 10^5$ m^{-1}, and $E \approx 3 \times 10^3$ V/m.

to focus on the influence of N_{dip} and N_{rep}. Note that these initial positions are on the same streamline, separated by 45°. The six basic types of behavior are as follows.

(1) Aligned rotating (Figure 3A, SI movie 3). The two dipoles align nearly vertically with the applied field and move in unison (approximately in circles) with a fixed distance between them. Because they are aligned vertically, the x-position for both dipoles is always approximately equal at any given time, yielding a distinctive positive slope in the phase plot (i.e., $x_1 \approx x_2$).

(2) Dual orbiting (Figure 3B, SI movie 4). The two dipoles orbit around each other on nearly identical trajectories that are mirror images of each other, yielding a distinctive negative slope in the phase plot (i.e., $x_1 \approx -x_2$). The dipoles are pulled near each other when they are close to aligned vertically but then repel when the flow aligns them horizontally. The resulting trajectories are shaped qualitatively like skewed ovals aligned at a 45° angle.

(3) Bicyclic orbiting (Figure 3C, SI movie 5). The two dipoles orbit around each other but periodically get pushed into and out of the region near the stagnation point in the center of the flow field. The corresponding phase plot is complicated but symmetric around the line $x_1 = -x_2$.

(4) Stagnating (Figure 3D, SI movie 6). One of the dipoles is pushed into the stagnation point, while the other orbits around it at approximately a fixed distance away. Because the dipole in the stagnation point always has $x_1 \approx 0$ while the other one is continuously moving, the phase plot has a characteristic flat slope.

(5) Wobbling (Figure 3E, SI movie 7). The trajectories here are similar to stagnating, except that both dipoles continue to orbit on different streamlines. Because they are moving at different velocities, the only predictable aspect of the phase plot is that the range of x_1 is greater than that of x_2 and that the phase plot trajectories qualitatively "wobble" about.

(6) Chasing (Figure 3F, SI movie 8). The two dipoles appear to "chase" each other on the same streamline (different from the streamline they started on), separated by a short distance about 45° apart. The phase plot has a characteristic circular shape.

Two other types of behavior, not shown in Figure 3, were also observed. For sufficiently strong repulsive forces and weak dipolar attraction, one or both of the dipoles moved outside the boundaries of the cellular flow (i.e., $|x| > \pi/2$, $y > \pi$, or $y < 0$). Qualitatively, the dipoles "pushed" one another out of the cellular flow region; we refer to this behavior as "expelled". A similar but distinct behavior was observed for larger magnitudes of N_{dip}, where the dipoles clearly aligned but moved in sufficiently large orbits that one or both of the dipoles moved periodically into and out of the domain. We denote this behavior as "aligned but expelled".

The numerical calculations revealed that the different behaviors are favored over particular ranges of N_{dip} and N_{rep}. A "phase diagram" of the steady-state trajectory behavior is shown in Figure 4, in which two key features are noteworthy. First, the aligned trajectories (blue diamonds) all occur on the lower right-hand side of the diagram, while all of the other "nonaligned" trajectories occur in the upper left-hand side of the diagram. This general trend is physically intuitive, since we expect the dipoles to remain aligned with the imposed electric field more readily for larger values of N_{dip}, but there is a sharp transition between aligned and nonaligned trajectories indicated by the dashed black line. Indeed, the existence of this sharp transition can be predicted in the context of the model. A balance of the radial components of the dipolar attraction and repulsive force requires

$$F_{dip} \approx F_{rep} \rightarrow \frac{N_{dip}}{{\rho_{eq}}^4} \approx \frac{N_{rep}}{{\rho_{eq}}^{13}} \rightarrow \rho_{eq} \approx \left(\frac{N_{rep}}{N_{dip}}\right)^{1/9} \qquad (12)$$

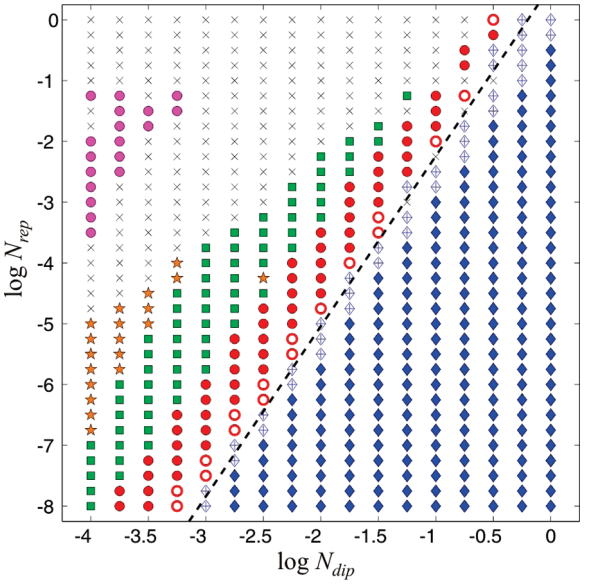

Figure 4. Phase diagram showing the steady-state trajectory behavior of two point dipoles in a two-dimensional cellular flow as a function of the dimensionless parameters N_{dip} and N_{rep}. The initial coordinates were $(x_1, y_1) = (\pi/4, \pi/2)$ and $(x_2, y_2) = (0, \pi/2)$ for each calculation. The symbols are black crosses = expelled from domain; solid blue diamonds = aligned rotating; hollow blue diamonds = aligned but ultimately expelled; solid red circles = dual orbiting; hollow red circles = bicylic orbiting; green squares = stagnating; orange stars = wobbling; and magenta circles = chasing. The dashed black line qualitatively separates aligned and nonaligned trajectories and has a slope of 14/5 (see text).

where ρ_{eq} is the separation distance at which the radial forces are balanced. Because the repulsive force has no angular component, a balance of the angular forces requires the dipolar force to be balanced by the fluid drag

$$F_{drag} \approx F_{dip} \rightarrow u_x \approx \frac{N_{dip}}{{\rho_{eq}}^4} \qquad (13)$$

Near the center of the cell the flow mimics a solid-body rotation, with **u** increasing linearly with distance from the stagnation point. Restricting attention to this vicinity, we have the approximation $u_x \approx \rho_{eq}$, and combination of eqs 12 and 13 yields the critical relation

$$N_{rep} \approx (N_{dip})^{14/5} \qquad (14)$$

The slope of the dashed black line in Figure 4 is exactly 2.8, in accord with eq 14. Similar arguments based on a torque balance yield the same result. Qualitatively, if the torque exerted by the dipolar interaction is sufficiently strong, the dipoles will remain aligned with the field, but if the fluid drag is strong enough, then the dipoles will rotate around each other. More generally, the critical transition will obey the relation $N_{rep} \sim (N_{dip})^{(m+1)/5}$ for any $m > 4$, suggesting that the existence of a transition between aligned and nonaligned trajectories is insensitive to the specific choice of power-law exponent (cf. eq 6).

Three-Dimensional Numerical Simulations

Many of the observed 2-D trajectories are distinctive, and a fascinating mathematical question is whether the complicated steady-state trajectories can be predicted analytically from the nonlinear governing equations. Indeed, many of the trajectories

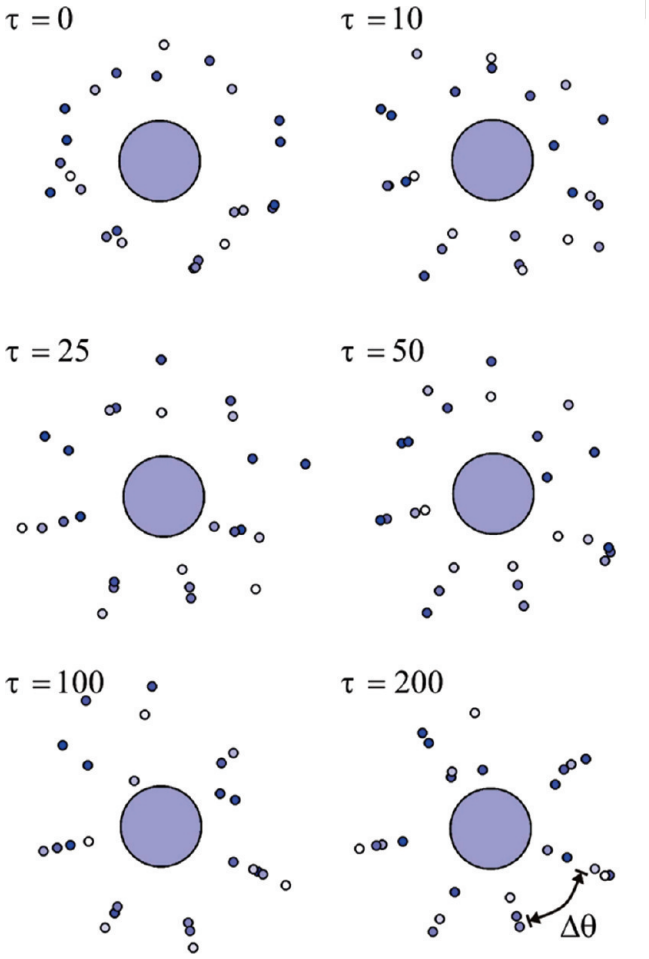

Figure 5. Numerically calculated sequence showing the projected (plan) view of 25 point dipoles, initially placed in random positions, undergoing dynamic angular segregation in a toroidal flow field. See also Supporting Information movie 9. Parameters: $N_{dip} = 10^{-2}$, $N_{rep} = 10^{-4}$, $\lambda L = 10$.

bring to mind the classical studies of particle dynamics via inverse power laws that yield epitrochoids and other parametric curves.[22] Here, however, we focus on whether the model can replicate any of the experimental observations. We therefore note the second significant feature in Figure 4, which is that there exists a broad swath of dimensionless parameters for which dual orbiting occurs (red circles). This result is noteworthy because dual orbiting is, at least qualitatively, the behavior most similar to that observed experimentally (cf. Figure 1).

Focusing on the regime of parameter space where dual orbiting occurs, we now extend the model to N interactions in a full three-dimensional flow field. As noted above, the three-dimensional toroidal flow is mimicked by extending the 2-D cellular flow profile in the z-direction with zero z-velocity, i.e., $\mathbf{u} = (u_x, u_y, 0)$, and imposing periodic boundary conditions at $z = 0$ and $z = \lambda L$ where λL is the dimensionless circumference of the large vesicle inducing the EHD flow. Although there is no fluid flow in the z-direction, particle motion in the z-direction is induced by the dipolar and repulsive interactions, which depend on the relative orientation of each particle pair (including the component in the z-direction).

Equation 7 was solved numerically for each of N particles. The results of a typical simulation are shown in Figure 5 where the position of 25 point dipoles, all with equal values of $N_{dip} = 10^{-2}$, $N_{rep} = 10^{-4}$, are tracked through time. The results are shown with a projected view (i.e., looking from the y-direction toward the $x-z$ plane) where the z-coordinate has been mapped onto an angular polar coordinate; the large blue circle is the resulting excluded zone and is intended to represent schematically the presence of the large vesicle generating the surrounding EHD flow. At $\tau = 0$, the point dipoles are all placed randomly throughout the domain. As they began moving in the flow field (see Supporting Information movie 9), they begin to align along preferred orientations. Bands are discernible as early as $\tau = 10$, and by $\tau = 200$ all but two of the dipoles are aligned along just six basic angular orientations. The tendency toward banding is quantified more precisely in Figure 6A, which plots the angular separation $\Delta\theta$ between every

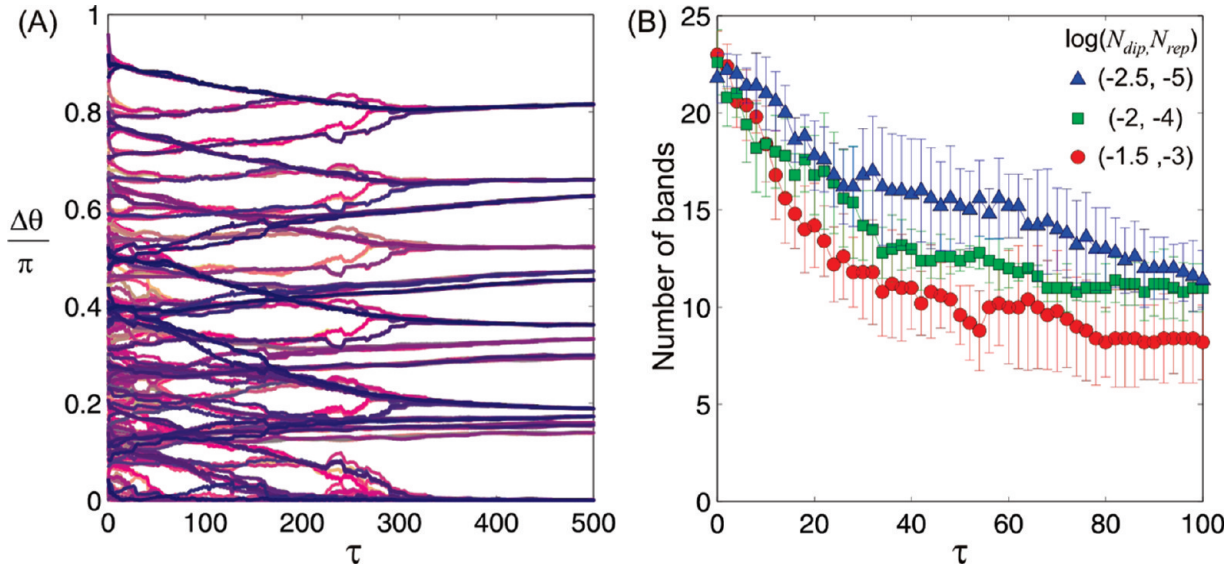

Figure 6. (A) Angular separation between each point dipole and the other 24 as a function of time, extracted from the same calculations as shown in Figure 5. Note the evolution from initially random to discrete angular separations, indicative of the banding phenomenon. The varied colors serve to differentiate each of the 300 curves. (B) Number of discrete bands, defined by a 1% tolerance in angular deviations, as a function of time for three different sets of parameters: triangles, $(N_{dip}, N_{rep}) = (10^{-2.5}, 10^{-5})$; squares, $(N_{dip}, N_{rep}) = (10^{-2}, 10^{-4})$; and circles, $(N_{dip}, N_{rep}) = (10^{-1.5}, 10^{-3})$. In each case, there were 25 initially randomly positioned dipoles and $\lambda L = 10$. Note that the number of discrete bands decreases more rapidly for larger values of N_{dip} and N_{rep}. Each curve is the mean of five simulations, and the error bars represent one standard deviation.

dipole and the other 24. The 300 individual curves rapidly condense into a much smaller subset of curves, reflecting the fact that many of the dipoles align onto the same angular orientation.

Calculations repeated with other random initial configurations, and other values of N_{dip} and N_{rep} revealed the same basic trend toward angular banding, provided N_{dip} and N_{rep} were chosen from the parameter space that corresponded to dual orbiting shown in Figure 4. Representative examples of the banding dynamics for different values of N_{dip} and N_{rep} are shown in Figure 6B. The "number of bands" is defined here as the number of nonempty intervals in the histogram of angular positions, with the interval width set as $\pi/100$ (i.e., a 1% tolerance in angular deviation). Note that this definition provides a conservative overestimate of the number of bands, since dipoles which "look" like they are in the same band might actually have more than a 1% deviation in angular position. The key observation in Figure 6B is that the number of discrete bands decreases in a manner qualitatively similar to that shown in Figure 5, although the rate of banding depends on the specific values of N_{dip} and N_{rep}. Not surprisingly, the band formation occurs more rapidly for larger values of N_{dip} and N_{rep} (again, provided the values correspond to the dual orbiting case in Figure 4). More importantly, the simulations show that the banding phenomenon is robust: qualitatively similar banding dynamics are observed for values of N_{dip} and N_{rep} that vary respectively by $1-2$ orders of magnitude.

Much more complicated behavior was observed for other parameter values, such as those corresponding to bicyclic orbiting. The main result here, however, is the strong similarity between the experimentally observed bands (Supporting Information movies 1 and 2) and the numerical calculations (Supporting Information movie 9), suggesting that the model of point dipoles moving in a circulatory flow indeed captures the salient physical features of the experimental system.

Conclusions

The primary conclusion from our study is that the observation of dynamic angular segregation of vesicles is consistent with a mechanism based on dipolar interactions. We showed that a simplified model based on point dipoles in a cellular flow yields a rich variety of trajectories, some of which closely mimic the experimental observation of dynamic angular segregation. Many questions remain, however. First, from an experimental perspective it is not clear why some of the large vesicles immediately displayed lifting versus orbiting, nor is it clear what triggered the transition between modes. Moreover, to our knowledge neither the lifting nor orbiting behaviors have been reported with polydisperse suspensions of rigid colloids, begging the question of why vesicles are apparently different. From a modeling perspective, several refinements to the model might begin to help address this question. For example, the 3-D modeling here focused on the case of all N dipoles having the same values of N_{dip} and N_{rep}, but experimentally these will all be different (due to the polydispersity of the vesicle suspension). Modeling could be performed where distributions in N_{dip} and N_{rep} are assigned to the orbiting vesicles. Likewise, in the current model the large vesicle simply generates the EHD flow, but in practice it also distorts the electric field; a more complicated model could incorporate a nonuniform electric field through the domain. There could also be smaller and transient EHD flow fields generated by the small vesicles themselves whenever they are in closer proximity to the electrode. The point-dipole model presented here can serve as a limiting case for future calculations that tackle these questions.

Acknowledgment. We thank the Harvard Nanoscale Science and Engineering Center for partial funding.

Supporting Information Available: Nine supplementary movies, including two experimental movies and seven movies of numerical simulations. This material is available free of charge via the Internet at http://pubs.acs.org.